[Co II(BPyPy COH)(OH)] 2+: A Catalytic Pourbaix Diagram and AIMD Simulations on Four Key Intermediates

Alberto, Roger ; Iannuzzi, Marcella ; Gurdal, Yeliz ; Probst, Benjamin

Abstract: Proton reduction by [CoII(BPyPy2COH)(OH2)2]2+ (BPyPy2COH = [2,2'-bipyridin]-6-yl-di[pyridin-2-yl]methanol) proceeds through two distinct, pH-dependent pathways involving proton-coupled electron transfer (PCET), reduction and protonation steps. In this account we give an overview of the key mechanistic aspects in aqueous solution from pH 3 to 10, based on electrochemical data, time-resolved spectroscopy and ab initio molecular dynamics simulations of the key catalytic intermediates. In the acidic pH branch, a PCET to give a CoIII hydride is followed by a reduction and a protonation step, to close the catalytic cycle. At elevated pH, a reduction to CoI is observed, followed by a PCET to a CoII hydride, and the catalytic cycle is closed by a slow protonation step. In our simulation, both CoI and CoII–H feature a strong interaction with the surrounding solvent via hydrogen bonding, which is expected to foster the following catalytic step.

DOI: https://doi.org/10.2533/chimia.2019.906

Originally published at:
Alberto, Roger; Iannuzzi, Marcella; Gurdal, Yeliz; Probst, Benjamin (2019). [Co II(BPyPy COH)(OH)] 2+: A Catalytic Pourbaix Diagram and AIMD Simulations on Four Key Intermediates. CHIMIA International Journal for Chemistry, 73(11):906-912.
DOI: https://doi.org/10.2533/chimia.2019.906

doi:10.2533/chimia.2019.906 Chimia 73 (2019) 906–912

$[Co^{II}(BPyPy_2COH)(OH_2)_2]^{2+}$: A Catalytic Pourbaix Diagram and AIMD Simulations on Four Key Intermediates

Roger Alberto[a], Marcella Iannuzzi[a], Yeliz Gurdal[b]*, and Benjamin Probst[a]*

Abstract: Proton reduction by $[Co^{II}(BPyPy_2COH)(OH_2)_2]^{2+}$ ($BPyPy_2COH$ = [2,2'-bipyridin]-6-yl-di[pyridin-2-yl]methanol) proceeds through two distinct, pH-dependent pathways involving proton-coupled electron transfer (PCET), reduction and protonation steps. In this account we give an overview of the key mechanistic aspects in aqueous solution from pH 3 to 10, based on electrochemical data, time-resolved spectroscopy and *ab initio* molecular dynamics simulations of the key catalytic intermediates. In the acidic pH branch, a PCET to give a Co^{III} hydride is followed by a reduction and a protonation step, to close the catalytic cycle. At elevated pH, a reduction to Co^{I} is observed, followed by a PCET to a Co^{II} hydride, and the catalytic cycle is closed by a slow protonation step. In our simulation, both Co^{I} and Co^{II}–H feature a strong interaction with the surrounding solvent *via* hydrogen bonding, which is expected to foster the following catalytic step.

Keywords: *Ab initio* Molecular dynamics · Cobalt polypyridyl · Density functional theory · Pourbaix diagram · Proton coupled electron transfer

Roger Alberto is full Professor for Inorganic and Radiochemistry at the University of Zurich since 2005. He studied chemistry at the ETH Zurich, and completed with a PhD on fluoro complexes of technetium in 1988. He then became Alexander von Humboldt Fellow at the TU Munich with Prof. W. A. Herrmann and at Los Alamos National Laboratory with Prof. A. Sattelberger, working on high-valent ^{99}Tc complexes. From 1991 to 1998 he was senior researcher at the Paul Scherrer Institute (PSI) in radiopharmacy with Prof. P. A. Schubiger. From 1999 he was Professor at the University of Zurich, and became full Professor in 2005. He had guest professorships at the NU Singapore with Prof. A. Hor and at the Ecole National Supérieur de Chimie in Paris with Prof. G. Jaouen. From 2006 to 2012 he was head of the Institute of Inorganic Chemistry and from 2013 to 2016 Director of the Department of Chemistry at the University of Zurich. Since 2013 he is head of the University Research Priority Project 'Light to Chemical Energy Conversion LightChEC'. He received an award for Excellence in Bioorganometallic Chemistry in 2006 and an Alexander von Humboldt Research Award 2017. He is a passionate collector of chemical elements and all kind of antique books.

Marcella Iannuzzi is Privatdozentin in Computational Materials Science at the University of Zurich since 2018. Her research field is the development and application of computational methodologies for the atomistic simulations of condensed matter. She has specialised in the investigation of complex interface systems, combining the accurate description of the interatomic interactions, including environment effects, with the sampling of the accessible phase space. She received her PhD degree in Materials Sciences from the University of Milano in 2001. Afterwards, she joined the group of Prof. Michele Parrinello as postdoctoral researcher, at the Max Planck Institut in Stuttgart (D) first, and later the ETH Zürich (CH). Between 2006 and 2009, she was hired in the group of Core and Fuel Behaviors in the department for Nuclear Energy and Safety, at the Paul Scherrer Institut (CH). Later, she came to the University of Zürich in the group of Prof. J. Hutter, where in 2012 she became Oberassistant.

Yeliz Gurdal is Assistant Professor in the Bioengineering Department at Adana Alparslan Turkes Science and Technology University (ATU), located in Turkey. Her current research concerns Density Functional Theory and *Ab initio* Molecular Dynamics investigation of molecular water reduction catalysts immobilized on semiconductor or metal surfaces as well as catalysts immersed in aqueous solution. Dr. Gurdal achieved her PhD degree in the Chemistry Department of University of Zurich, Switzerland, where she also acquired a postdoctoral experience. Following, she joined SASA Polyester, an industrial company located in Turkey, and she contributed to the establishment of SASA R&D Department.

*Correspondence: Dr. B. Probst[a], E-mail: benjamin.probst@uzh.ch, Asst. Prof. Dr. Y. Gurdal[b], E-mail: ygurdal@atu.edu.tr
[a]Department of Chemistry, University of Zurich, Winterthurerstrasse 190, CH-8057 Zurich; [b]Department of Bioengineering, Adana Alparslan Turkes Science and Technology University, Catalan Caddesi 201, Saricam, Adana, Turkey

Benjamin Probst is Senior Research Associate in the Group of Prof. Roger Alberto, University of Zurich. His research interests centre on the topic of artificial photosynthesis and solar fuels. He supervises the synthesis of novel, first row transition metal-based water-reduction catalysts and photosensitisers. He is closely involved in mechanistic investigations including electrochemical and (time resolved-) spectroscopic methods. Dr. Probst obtained his PhD degree in 2010 from the University of Zurich, with a thesis entitled 'Photocatalytic Hydrogen Production'. He then moved to Andreas Borgschulte at EMPA in Dübendorf for a postdoctoral stay to work on the Sabatier reaction. In 2013 he joined the URPP LightChEC at the University of Zurich as a Research Associate.

1. Introduction

Major restructuring of the world energy sector lies ahead in this century, if global warming is to be limited well below 2 °C above the preindustrial level, as agreed in the Paris Agreement 2015, signed by 195 nations up to now.[1] Effectively, this can only be accomplished if the exponential growth in the share of renewable energies, as seen in the last decade, continues and fossil fuels phase out by 2050.[2] As renewable energies like sun and wind are of intermittent nature, energy storage, *e.g.* in the form of chemical bonds, will be a major prerequisite to achieve this transition.[3] Hydrogen, obtained from water electrolysis will likely serve as a key intermediate in a post-fossil future.[4] Today, water electrolysis can be roughly subdivided into three technologies according to the charge carrier in the membrane: proton-exchange membrane (PEM; protons from anode to cathode); alkaline electrolysers (hydroxide ions from cathode to anode) and solid oxide electrolysers (SOE; oxide ions from cathode to anode).[5] Alkaline electrolysis can be considered the most mature technology, with units in the MW range, and SOE and PEM electrolysers are considered in the R&D and demonstration phase, respectively.[5a] Even though very high current densities, low cold start up-times and high-pressure operation are in principle possible with PEM electrolysers, large-scale employment is limited by the short stack lifetime and high capital costs for deployment.[5a,b] Research for alternative electrocatalysts for PEM electrolysers is thus highly desirable.

As seen with the advancement PEM electrolysis by the invention of polymer-based electrolytes for acidic electrolysis in the 1960s,[6] molecular catalysts for both oxidation and reduction of water can in principle allow for a reduction of catalyst load, fine tuning of catalytic properties and stabilities and thus lowering of capital costs. For hydrogen production, first transition row metal catalysts based mainly on iron, nickel, cobalt and molybdenum have been intensively investigated.[7] Since early reports on proton reduction on cobalt bipyridine, cobaloxime and related macrocyclic structures in the 1980s,[7g,8] featuring turnover numbers (TON) in the range of 10–100 in water, significant improvements have been observed using cobalt polypyridyl-type catalysts in the last decade,[7a,9] with state of the art catalysts reaching close to 100 kTON in neutral, aqueous solution,[9f] albeit at usually 400 mV and higher overpotentials.[7c,g,9j] Optimisation of rate and catalytic potential, whilst maintaining the high stability, represents the major drive for this class of catalysts. Only by profound knowledge of molecular mode of action in catalysis can improved properties be rationally achieved.

This account of research thus focuses on the mode of action of a prototype cobalt polypyridyl catalysts: $[Co^{II}(BPyPy_2COH)Br_2]$ ($BPyPy_2COH$ = [2,2'-bipyridin]-6-yl-di[pyridin-2-yl]methanol). $[Co^{II}(BPyPy_2COH)Br_2]$ was one of the first cobalt polypyridyl catalysts described in the literature in 2013.[9d] It features a methanol bridgehead for solubility, substituted with two pyridyl and one 2,2'-bipyridyl substituent, providing a tetradentate ligand to cobalt. The remaining two coordination sides are occupied by a closely and a very weakly bound bromide ion (2.49 resp. 2.79 Å),[9d] both of which are replaced by solvent water molecules upon dissolution.[10] It allows for up to 9 kTON of H_2 in a photocatalytic assay with the $[Re(py)(CO)_3bipy](OTf)$ photosensitizer (Re-PS, OTf^- = trifluoromethanesulfonate), and ascorbic acid as sacrificial electron donor in pH 4 aqueous solution.[9d] Immobilisation of the catalyst on a polymer resin allowed a recycling of the catalyst.[9d] A detailed kinetic analysis at pH 8 revealed the individual steps for hydrogen production in 2015,[10] and a follow-up investigation in 2016 shed light on the catalysis in a system using quinones and TCEP (tris-(2-carboxyethyl)-phosphine) as electron relay/donor system.[11] In 2017, an electrochemical investigation established the mechanism from pH 3 to 10.[9j] In the following, the previous results are summarized along with a new set of calculations performed for all identified catalytic intermediates in an explicit solvation model, shining light on key catalytic reaction steps.

2. Results and Discussion

We propose, as outlined in the following, that reduction of the archetypic $[Co^{II}(BPyPy_2COH)(OH_2)_2]^{2+}$ (Co^{II}) for hydrogen production follows two distinct pathways, depending on the pH of the media (Scheme 1). A fast pathway is identified in the pH domain below 7, starting with proton coupled electron transfer (PCET), to give $[Co^{III}(BPyPy_2COH)(OH_2)H]^{2+}$ (Co^{III}–H), followed by electron transfer to $[Co^{II}(BPyPy_2COH)(OH_2)H]^{+}$ (Co^{II}–H), which is irreversibly protonated to give back Co^{II} and H_2. At pH above 7, a much slower mechanism is at work, and hydrogen production competes with decomposition of the catalyst. This mechanism is thought to proceed through reduction of Co^{II} to $[Co^{I}(BPyPy_2COH)(OH_2)]^{+}$ (Co^{I}), followed by PCET to (Co^{II}-H). The latter has a $pK_a < 3$, making protonation in neutral to basic media extremely slow, potentially limiting the catalytic turnover due to deleterious hydride transfer to the organic ligand framework.

In the next three sections an account of the work that led to the mechanistic proposal will be given, including results obtained from electrochemistry in water, as a function of pH, and

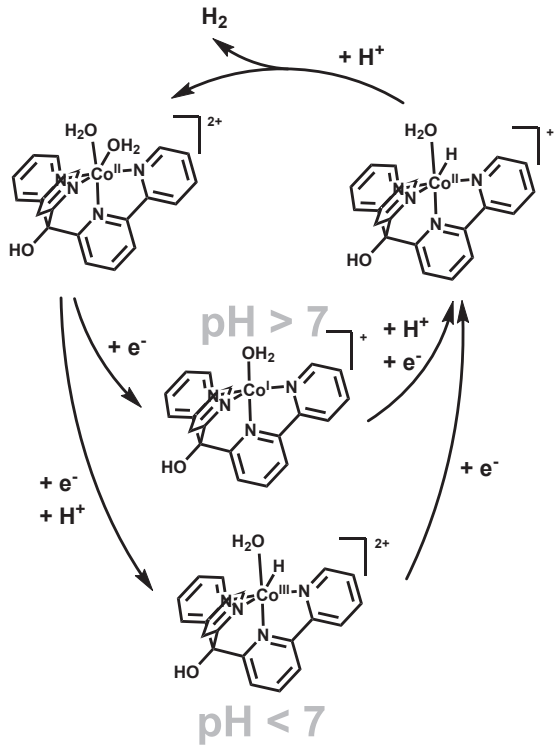

Scheme 1. Proposed catalytic cycle.

time-resolved spectroscopy in water using rhenium- and/or ruthenium-type photosensitizers with either triethanolamine (TEOA) or ascorbic acid (AscOH) as electron donors. The experimental results are complemented by a theoretical study based on the atomistic modelling of four key intermediates of the catalytic cycle within explicit solvent, where correlations between structural dynamics and electronic properties are discussed.

2.1 *Electrochemistry*

In the following the electrochemistry of $[Co^{II}(BPyPy_2COH)(OH_2)_2]^{2+}$ (Co^{II}) in different electrolytes is discussed in detail, and the conclusions are visualized in a catalytic Pourbaix diagram. Reduction of $[Co^{II}(BPyPy_2COH)Br_2]$ in organic solvent (DMF, 100 mM $TBAPF_6$) gives a reversible wave at –1.49 V vs Fc/Fc^+ (see Fig. SI 1 in the Supplementary Information), which is readily assigned to the $Co^{II/I}$ couple based on previous studies.[9c,10] A second, irreversible wave follows with a cathodic peak potential (E_{pc}) of –2.23 V vs Fc/Fc^+. No oxidation could be observed within the potential window accessible in this experiment. In aqueous media, containing 100 mM LiOTf as electrolyte, a quasi-reversible wave is observed at –0.91 V vs NHE (D(300 K) = 4.5 × 10^{-6} cm^2s^{-1}; Fig. SI 2), displaying the characteristic shape for surface grafting.[12] Fast dissolution upon re-oxidation is implied by concentration- and scan rate dependencies.[9j] This wave is assigned to the $Co^{II/I}$ couple, in analogy to the experiments in DMF. No further redox chemistry is visible in the potential window accessible to the experiment, nor is there any sign of catalytic proton reduction by the so formed Co^I.

In contrast, when a buffered aqueous electrolyte was employed (40 mM each AcOH, H_3PO_4, $B(OH)_3$, Britton-Robinson Buffer, BRB; 100 mM LiOTf, Fig. 1), the electrochemistry changes significantly: up to pH 7 a quasi-reversible, pH dependent wave is observed with an intercept of –0.53 V vs NHE at pH 0 and a slope of 54 mV/pH unit. This first peak is followed by a second, quasi-reversible and pH independent peak at –0.93 V vs NHE, displaying an exponential peak current increase with pH (Fig. SI 3), indicative for catalysis. Above pH 9.5 a cathodic shift with 50 mV/pH of the second reduction was observed.

In the pH range up to 7, the first, pH-dependent couple is consistent with a PCET from the initial Co^{II} to a Co^{III}–H, followed by a pH-independent, catalytic wave, which is assigned to the reduction of Co^{III}–H to Co^{II}–H. Above pH 9.5, a deprotonation of the aquo ligands bound to the Co^{II} occurs. This is consistent with the observed cathodic shift of the reduction and the pK_a of 9.39 ± 0.1 for Co^{II} determined independently by spectroscopy (Fig. SI 4). LSV experiments were performed with GC-TCD in-line probing to confirm the catalytic hydrogen production as outlined above (Fig. SI 5). Indeed a drastic increase in both hydrogen production and current was observed at –0.93 V vs NHE, from pH 7 to 2, along with a decrease in onset potential (pH 2: –0.56; pH 4: –0.69 and pH 7: –0.88 V vs NHE). This interpretation is consistent with a catalytic Pourbaix diagram as outlined below (Fig. 2). It implies that H_2 formation occurs from a Co^{II}–H by protonation. Since no pH dependency of the catalytic wave at –0.93 V vs NHE was found, the pK_a of the Co^{II}–H/Co^{II}–H_2 couple is below 3, and H_2 formation is owed to the irreversible loss of H_2 from Co^{II}-H_2 formed in equilibrium with Co^{II}–H. At pH above 7 H_2 formation is slowed down significantly due to said equilibrium, in line with the decrease in current and hydrogen production rate observed in LSV experiments (Fig. SI 5). One implication of the analysis is a very narrow range (pH 7 – 7.25) where direct, two electron/one proton reduction of Co^{II} to Co^{II}–H occurs. Between pH 7.25 and 9.4 reduction of Co^{II} to Co^I occurs, followed by a PCET to Co^{II}-H. Above pH 9.4, deprotonation of Co^{II} to Co^{II}–OH occurs, which reduces to Co^I in a PCET. The formation of Co^{II}–OH was shown to be partially irreversible by titration experiments, likely due to decomplexation and formation of cobalt oxide.[13]

2.2 *Time-resolved Spectroscopy*

The reaction sequence Co^{II} to Co^I, followed by PCET to Co^{II}–H and protonation to give Co^{II} and H_2 at around pH 8 was determined independently by a combination of time-resolved techniques in 2015.[10] Upon excitation of the $[Re(py)(CO)_3bpy](OTf)$ dye (Re-PS) Rodenberg *et al.* found reductive quenching by triethanolamine (TEOA) to give Re-PS^- with k_q = 5.1 × 10^7 $M^{-1}s^{-1}$, and a cage escape yield of 0.75. The highly reducing Re-PS^- (–0.94 V vs NHE) is intensely blue, with bands at ~470 nm and ~850 nm. In the absence of an electron acceptor, Re-PS^- has a lifetime in the upper microsecond range, before decomposition occurs with concomitant formation of hydrogen.

Co^{II}, on the other hand, shows two intense bands at 250 and 305 nm, originating from π–π* transitions of the $BPyPy_2COH$ ligand, and only weak bands in the visible. Co^I, generated by chemical reduction by decamethylcobaltocene in dry DMF, fea-

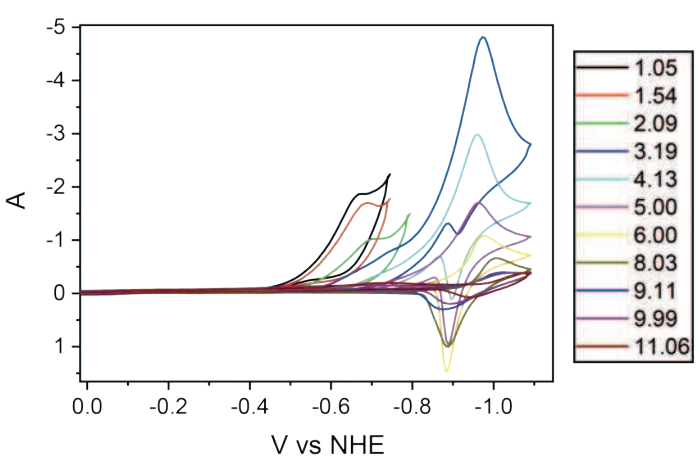

Fig. 1. Cyclic voltammetry on $[Co^{II}(BPyPy_2COH)Br_2]$ (1 mM) in 40 mM BRB, 100 mM LiOTf, 100 mV/s, pH adjusted with 2 M NaOH, referenced to NHE with $[MV]Cl_2$, WE = Hg, CE = Pt, RE = Ag/AgCl.

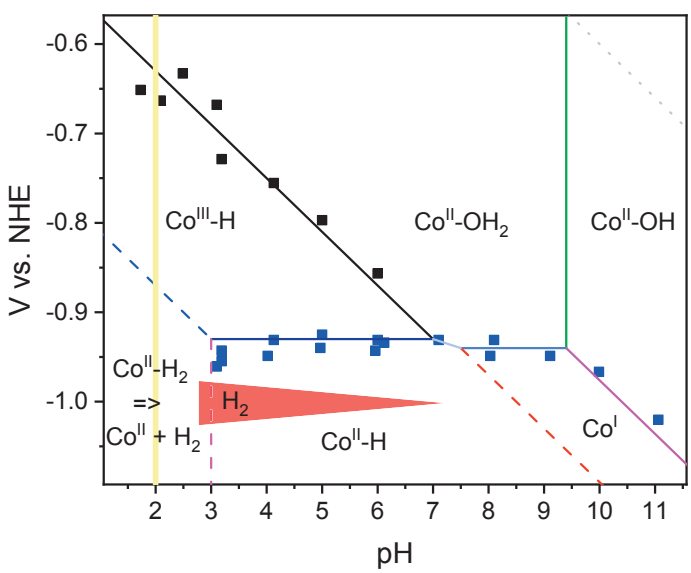

Fig. 2. Catalytic Pourbaix diagram summarising data from Fig. 1 and Figs SI 1 to SI 5 in the Supplementary Information. Black and blue dots: reduction potentials determined from cyclic voltammetry with 1 mM $[Co^{II}(BPyPy_2COH)Br_2]$, 2 or 40 mM BRB, 100 mM LiOTf, varying scan speeds, pH adjusted with 2 M NaOH, referenced to NHE with $[MV]Cl_2$, WE = Hg, CE = Pt, RE = Ag/AgCl; green and yellow line: titration experiment (Fig. SI 4); red triangle: H_2 evolution confirmed with CV and LSV with in-line GC (Fig. SI 3 and SI 5)); blue, black and magenta solid lines: guide for the eye; dashed lines: proposed redox/protonation processes; grey dotted: thermodynamic H^+ / H_2 couple.

tures a broad, intense absorption in the visible with a maximum at 638 nm ($\varepsilon = 5300\ M^{-1}\ cm^{-1}$). Formation of Co^{I} in a system with Re-PS and TEOA at pH ~8 could thus be confirmed by laser flash photolysis spectroscopy: upon formation of the characteristic $Re\text{-}PS^{-}$, prompt electron transfer to Co^{II} to give Co^{I} is observed, with a rate of $1.7 \times 10^{9}\ M^{-1}s^{-1}$, in line with experiments at lower pH.[9d] Under catalytically relevant concentrations (μM range) Co^{I} is thus formed on a timescale of μs. More interestingly, at pH ~8, Co^{I}, and no other species, is observed until a time range of several seconds, as opposed to the system at lower pH, using ascorbic acid as electron donor instead of TEOA, where the decay of Co^{I} occurs much faster and is a mixture of back reactions with oxidised ascorbate and H_2 formation.[9h,10,11,14] The decay of Co^{I} in this late time range was found to depend both on its initial concentration and on the pH. Good agreement was found in a global fit of the data at different [Co^{I}] and [H^{+}] when protonation to Co^{III}–H was considered to be a fast pre-equilibrium, followed by reduction to Co^{II}–H through the only electron donor left in solution, Co^{I}. At no time is there any accumulation of significant concentrations of Co^{III}–H, meaning that the process is best described as a PCET from Co^{I} to Co^{II}–H. Hydrogen evolution then occurs by protonation of so generated Co^{II}–H, with $2.2 \times 10^{7}\ M^{-1}s^{-1}$. To sum up, at pH around 8, Co^{II} is reduced to Co^{I}, which undergoes PCET to Co^{II}–H, which gives H_2 by relatively slow protonation.

2.3 *Calculations*

Ab initio molecular dynamics (AIMD) simulations with an integration time step of 0.5 fs are carried out for the catalyst within a fully explicit solvent environment in a cubic simulation cell containing 215 water molecules. The initial equilibration is carried out by 20 ps at constant ambient pressure and temperature (NPT ensemble), followed by 15 ps at constant volume and temperature (NVT ensemble). All simulations are carried out with the CP2K/QUICKSTEP package.[15]

Fig. 3a illustrates the ball and stick sketch of the optimized $[Co^{II}(BPyPy_2COH)(OH_2)_2]^{2+}$ consisting of one bipyridyl unit with two pyridine nitrogen atoms labelled as N_{Rpy1} and N_{Rpy2}, two pyridyl donors, labelled as N_{Lpy1} and N_{Vpy1}, and one hydroxy function in the backbone. The optimized catalyst in vacuum displays a non-ideal octahedral coordination. The strongly distorted structure is in line with X-ray diffraction analysis of $[Co^{II}(BPyPy_2COH)Br_2]$.[9d] Co–N distances vary from 2.4 Å to 2.9 Å, corresponding to binding interactions, where the lateral nitrogen, N_{Rpy1}, is the closest to the cobalt centre. There are two water molecules coordinating to $[Co^{II}(BPyPy_2COH)(OH_2)_2]^{2+}$ which can be also considered as binding, with Co–O_{water1} and Co–O_{water2} distances being 2.07 and 2.33 Å, respectively.

Separate AIMD runs have been carried out for the catalyst merged in the explicit water solvent, considering different intermediate states of the catalytic cycle. We modelled the initial state of the catalyst (Co^{II}) and the intermediates formed by the subsequent introduction of additional electrons and protons in the following order: first reduction (Co^{I}), first protonation (Co^{III}–H), second reduction (Co^{II}–H), and second protonation (Co^{II}–H_2).

Along the AIMD trajectory of the catalyst in its initial state two water molecules remain constantly coordinated to the cobalt centre, with average Co–O_{water1} and Co–O_{water2} distances oscillating around the values calculated for the optimised catalyst in vacuum. The average distances between the pyridine nitrogen atoms and cobalt range between 2.06 and 2.13 Å, Co–N_{Rpy1} again being the shortest one.

As discussed by Rodenberg *et al.*,[10] the first electron injection to $[Co^{II}(BPyPy_2COH)(OH_2)_2]^{2+}$ results in a penta-coordinate state ($BPyPy_2COH$ plus one water) with two possible spin multiplicities, either singlet or triplet. We consider both spin states in our AIMD simulations. In the triplet spin state, *hs*-$[Co^{I}(BPyPy_2COH)(OH_2)]^{+}$, O_{water1} preserves its position fluctuating around 2.23 Å from the cobalt centre and the distance between the near-

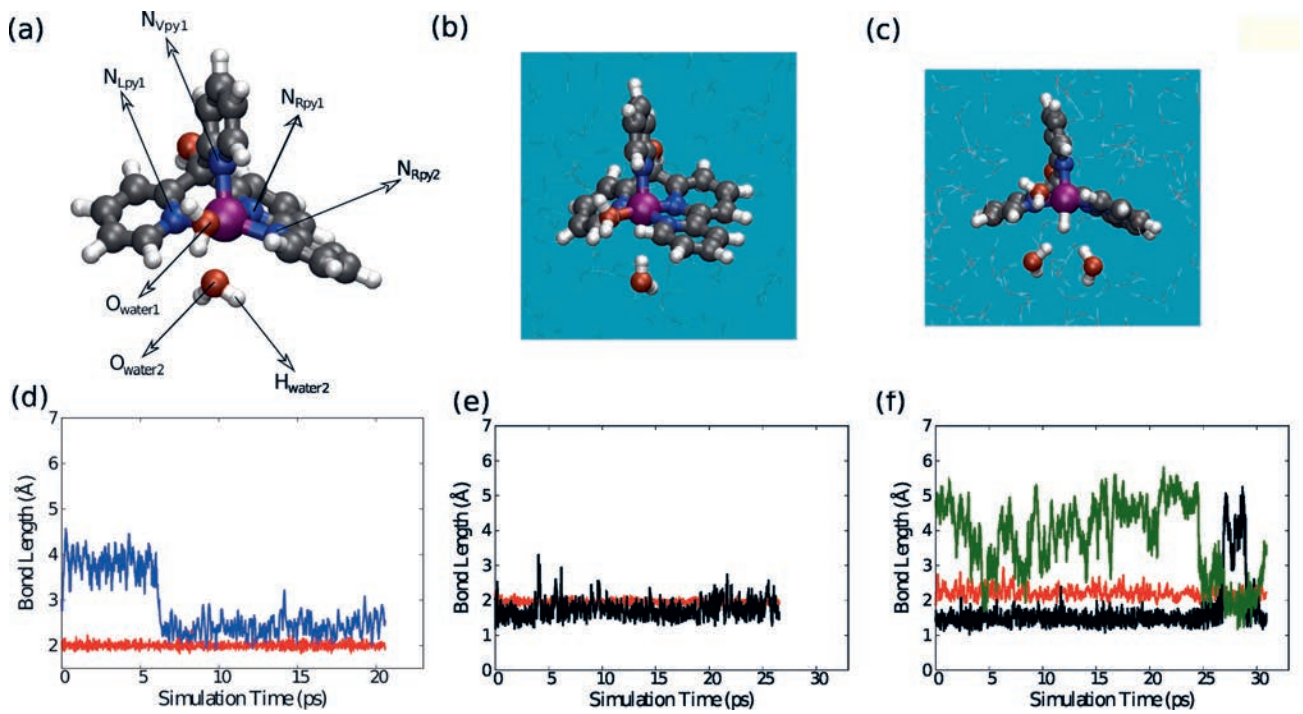

Fig. 3. (a) Ball and stick representation of $[Co^{II}(BPyPy_2COH)(OH_2)_2]^{2+}$. The nitrogen atoms in the pyridyl rings are labelled as N_{Lpy1}, N_{Lpy2}, N_{Rpy1}, N_{Rpy2}, and N_{Vpy1}. The oxygen belonging to the closest water molecule to the cobalt centre is labelled as O_{water1}, while the oxygen and hydrogen of the second closest solvent molecule are labelled O_{water2} and H_{water2}, respectively. (b) and (c) show selected snapshots of Co^{I} (singlet spin state) and the Co^{II}-H state taken at a simulation time of 17 ps and 26 ps, respectively. Colour code: grey: C, white: H, purple: Co, blue: N, and red: O. Water molecules under consideration are depicted with solid-coloured ball and stick representation. Solvent molecules are depicted using line representation. (d) $d_{Co\text{-}Owater1}$ (red) and $d_{Co\text{-}Hwater2}$ (blue) distances along the AIMD trajectory for the singlet spin state of Co^{I}. (e) $d_{Co\text{-}Owater1}$ (red), $d_{Hcobalt\text{-}Hwater2}$ (black) distances measured for the Co^{III}–H state. (f) $d_{Co\text{-}Owater1}$ (red), $d_{Hcobalt\text{-}Hwater2}$ (black), and $d_{Hcobalt\text{-}Hwater3}$ (green) distances measured for Co^{II}–H state.

est solvent H and the cobalt centre, $d_{Co\text{-}Hwater2}$, is relatively long, fluctuating around 3.42 Å. In the singlet spin state, we observe a significant rearrangement in the first solvation shell, where the second closest water molecule rotates such that H_{water2} points towards the cobalt centre. The structural change is clearly identified by the sudden shortening of $d_{Co\text{-}Hwater2}$, from 3.8 Å to 2.5 Å, already after 5 ps of simulation time (Fig. 3b, d). Clearly, the hydrogen bonding network, which connects the cobalt centre with the bulk solvent, is altered upon electron injection. We interpret this observation as the first step towards the formation of Co^{III}–H, the oxidative addition of H^+ to Co^I through protonation of the filled d_z^2 orbital at the cobalt (*vide infra).* The reaction can, however, not proceed here, as formation of Co^{III}–H would create an OH^-, the stabilisation of which would be associated with too high an energy penalty in a box of 215 molecules of H_2O (pH > 13). To proceed to the next step, we adapt the model starting a new trajectory from the obtained configuration of the catalyst in the singlet spin state, adding one proton close to the Co^I. Monitoring the trajectory we show the formation of a stable cobalt hydride, Co^{III}–H, with a bond length oscillating around 1.48 Å, while the next closest water hydrogen is at about 1.74 Å from the hydride, $d_{Hcobalt\text{-}Hwater2}$ (Fig. 3e).

The next trajectory is generated after adding one electron to the cobalt hydride, the second electron injection, to obtain Co^{II}–H. The resulting spin state is a doublet and the catalytic system is expected to become more prone to grab a proton from the solvent to form H_2. Indeed, the $d_{Hcobalt\text{-}Hwater2}$ distance becomes shorter, *i.e.* 1.48 Å and other water molecules approach the metallic centre. For instance, between 25 and 30 ps, we observe first the coordination of a second hydrogen to Co^{II}–H followed by an exchange of the coordinated water molecule, as evident from the plotted $d_{Hcobalt\text{-}Hwater2}$ and $d_{Hcobalt\text{-}Hwate3}$ in Fig. 3f. This dynamic behaviour is consistent with a flexible solvation shell around the Co^{II}–H which allows rearrangement in the hydrogen bond network and should favour the transfer of a proton. The very mobile and short-lived hydrogen bonding network close to the cobalt centre might confirm experimental observations that the second protonation is the rate-limiting step for H_2 production with $[Co^{II}(BPyPy2COH)(OH_2)_2]^{2+}$. As in the previous case, we need to add a proton to the simulation cell in order to model the proton transfer and observe the formation of molecular hydrogen. As a matter of fact, as soon as the proton is in the vicinity of Co^{II}–H, H_2 is released, the catalytic cycle is closed and the system spontaneously returns back to its initial state.

In order to correlate the structural dynamics with relevant electronic structure properties, we did monitor the frontier orbitals along the different trajectories obtained for the discussed intermediate states. This analysis has been performed for selected snapshots at a higher level of theory, *i.e.* PBE0-rVV10. Visualisations of the highest occupied (HOMO) and the lowest unoccupied (LUMO) molecular orbital distributions for representative snapshot's of each intermediate are displayed in Fig. 4. The HOMO of $[Co^{II}(BPyPy_2COH)(OH_2)_2]^{2+}$ is located on the cobalt centre, on all the pyridyl nitrogen atoms, and on the oxygen atoms of the closest water molecules. The corresponding LUMO is located on the bipyridine rings, but not on the cobalt centre. This suggests that a ligand-centred electron transfer should occur during the first reduction reaction. In the singlet spin state of the Co^I intermediate the main contribution to the HOMO arises from the cobalt centre, while some contributions appear on the bipyridine ring and N_{Vpy1}. Clearly, a d_z^2-like orbital is visible pointing in the direction of the Hwater2. The LUMO is mainly localised on the bipyridine ring. Following the first protonation reaction, in the Co^{III}–H intermediate, the HOMO is distributed almost over all the catalyst including solvent water molecules. The LUMO is localised on the bipyridine ring, which again suggests a ligand-assisted process for the second reduction reaction. The HOMO of Co^{II}–H is distributed on both the cobalt centre and the bipyridine unit. The LUMO is more prominently localised over lateral and vertically pyridine rings. Spin density analysis are carried out only

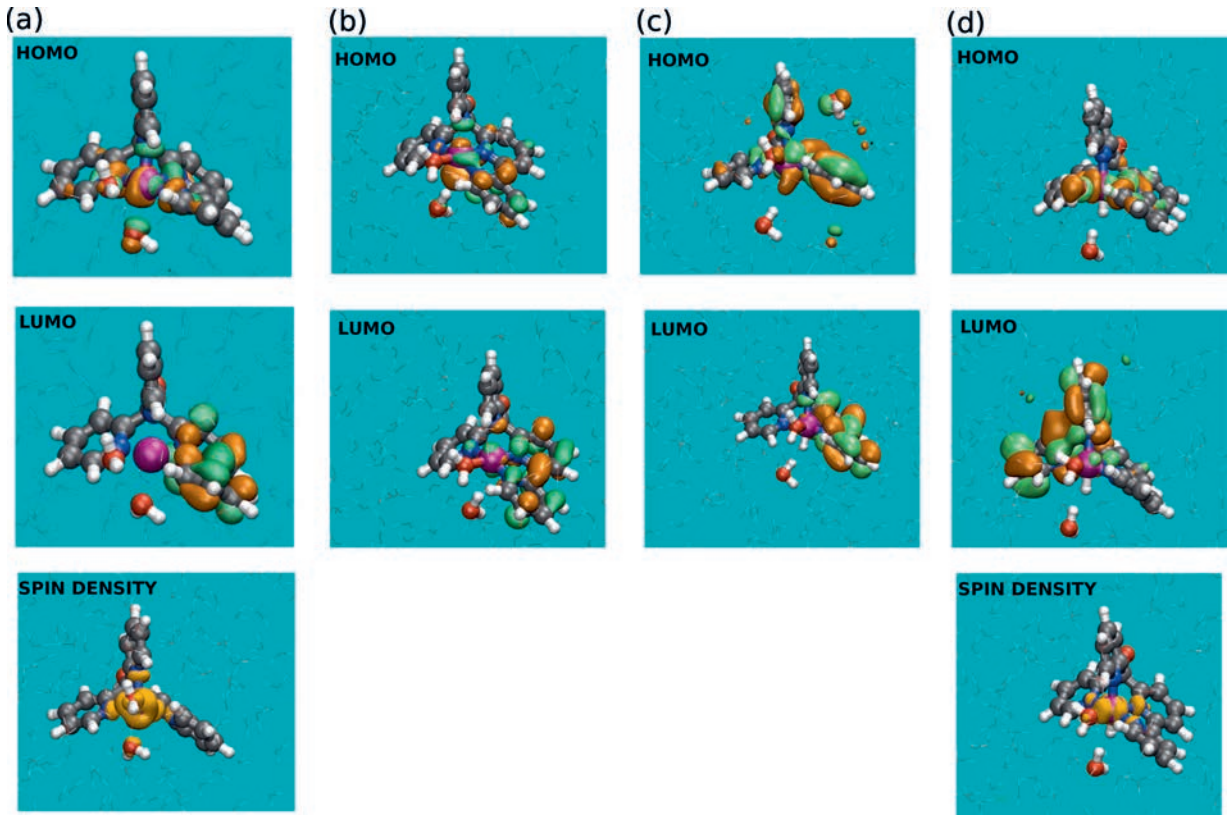

Fig. 4. HOMO and LUMO representations for (a) initial state of the catalyst (Co^{II}) at 18 ps, (b) Co^I at 20 ps, (c) Co^{III}–H at 25 ps, and (d) Co^{II}–H at 20 ps. Isosurfaces (orange for positive and green for negative) are set to ±0.024 e/Å^3. Spin densities are plotted only for Co^{II} and Co^{II}–H states, where isosurfaces are set to 0.002 e/Å^3.

for Co^{II} and Co^{II}–H states, having doublet spin states, as shown in the lowest panel in Fig. 4a and d. While the spin density of Co^{II} is localised on the cobalt centre, the closest water molecule, and all the pyridine N atoms, Co^{II}–H state has its spin density distributed over the cobalt centre, the closest water molecule and only laterally positioned N atoms.

Our analysis thus suggests that Co^{II} is reduced to a singlet Co^{I}, likely through a triplet Co^{I} state, which has a similar energy as the singlet state, but possibly represents a barrier to the reaction. The singlet state allows for protonation of the d_{z^2} orbital. This is visualised by a relatively short Co–H hydrogen bond of 2.5 Å. Prompt formation of Co^{III}–H is observed upon the addition of a proton to the singlet Co^{I}, with a Co–H bond of 1.48 Å. The next proton is found at 1.75 Å from the hydride, which reduces to 1.48 Å upon reduction to Co^{II}–H. Despite the short $d_{Hcobalt\text{-}Hwater}$ distance, Co^{II}–H displays some flexibility in its hydrogen bonding network. Upon addition of a second proton prompt formation of H_2 and Co^{II} is observed.

3. Outlook and Conclusions

In summary we find two distinct pathways for hydrogen production catalysed by $[Co^{II}(BPyPy_2COH)(OH_2)_2]^{2+}$. Below pH 7, Co^{II} is undergoing a PCET to Co^{III}–H, as evidenced by electrochemistry, followed by reduction to Co^{II} and subsequent protonation to give back Co^{II} and H_2. Above pH 7, reduction to Co^{I} is followed by a PCET to Co^{II}–H, as evidenced by time-resolved spectroscopy, followed by slow protonation to give back Co^{II} and H_2. In both cases, the last protonation step, *e.g.* protonation of Co^{II}–H, seems to be rate limiting. Electrochemical analysis suggests that the pK_a of Co^{II}–H lies below 3. Thus, H_2 formation is owed to the irreversible dissociation of Co^{II}–H_2 formed in equilibrium with Co^{II}–H and H^+ into Co^{II} and H_2. As for Co^{I}, an estimate for the pK_a of 7.25 is obtained from electrochemical analysis. As found by MD simulations, both triplet and singlet configurations for Co^{I} are possible, and lay energetically very close together. Molecular orbital analysis of Co^{II} implies that reduction goes into the bipyridyl fragment of the $BPyPy_2COH$ ligand, likely giving rise to the triplet configuration. Thus conversion to the singlet, required for protonation, might impose a barrier to the reaction. Based on LSV with concomitant H_2 detection an overpotential of 430 mV is estimated for H_2 production using $[Co^{II}(BPyPy_2COH)(OH_2)_2]^{2+}$.

Future catalysts based on the cobalt polypyridyl platform must therefore attempt to lower the overpotential, and possibly increase the rate for H_2 production. The former implies a lowering of the Co^{III}–H/Co^{II}–H couple, whereas the latter suggests an increase in the Co^{II}–H pK_a. Likely, however, the two parameters are coupled: electron-accepting ligands would lower the overpotential, but decrease the pK_a, and vice versa.[16] The strategy followed in this laboratory consists therefore in lowering the overpotential using electron-accepting ligands, whilst influencing the rate of protonation by using intramolecular proton relays.

4. Experimental

Information on the synthesis, electrochemical setup, the inline GC-TCD setup and additional data can be found in the supplementary information at *https://www.ingentaconnect.com/content/scs/chimia*

4.1 *Computational Details*

Electronic structure calculations are performed using hybrid Gaussian and plane wave basis set formalism of Kohn-Sham Density Functional Theory (DFT) implemented in CP2K/QUICKSTEP package.[15] Goedecker–Teter–Hutter pseudo potentials are used in order to describe the interaction between the valence electrons and the atomic cores.[17] The valence shells contain 17, 6, 4, 1, and 5 electrons for Co, O, C, H, and N, respectively. The molecular orbitals of all atomic kinds are expanded using double-zeta plus polarization basis sets which are optimized on molecular geometries (Mol-Opt method, m-DZVP).[18] The valence electron density in reciprocal space is described using auxiliary plane wave basis and its cut off is set to 400 Ry. Periodic boundary conditions and spin polarization are always applied. All geometry optimizations of the catalysts in vacuum and AIMD runs for the catalysts/water systems are performed using the general gradient approximation (GGA) by Perdew-Burke-Enzerhof (PBE).[19] Dispersion interactions are included via the nonlocal electron correlation scheme conceived by Vydrov and Van Voorhis, in the revised form (rVV10).[20] All post-processing analysis including frontier molecular orbital representations and spin density distributions are determined applying PBE0 hybrid density functional[21] with a 0.25 fraction of exact exchange, still augmented by the rVV10 electron correlation. As a summary of the simulation strategy, we carry out AIMD runs at the PBE-rVV10 level of theory and refine the electronic structures at the PBE0-rVV10 level.

Acknowledgements

For financial support of this work, we are grateful to the Swiss Science Foundation (Singergia Project CRSII2_160801/1) as well as to the University of Zurich through University Research Priority Program (URPP) LightChEC. We acknowledge PRACE for awarding us access to Marconi at CINECA, Italy.

Received: September 16, 2019

[1] UNFCC, Paris Agreement, **2015**.
[2] a) J. Rockstrom, O. Gaffney, J. Rogelj, M. Meinshausen, N. Nakicenovic, H. J. Schellnhuber, *Science* **2017**, *355*, 1269, DOI: 10.1126/science.aah3443; b) C. McGlade, P. Ekins, *Nature* **2015**, *517*, 187, DOI: 10.1038/nature14016.
[3] a) M. R. Shaner, S. J. Davis, N. S. Lewis, K. Caldeira, *Energ. Environ. Sci.* **2018**, *11*, 997, DOI: 10.1039/c8ee90019a; b) N. S. Lewis, D. G. Nocera, *Proc. Natl. Acad. Sci. USA* **2006**, *103*, 15729, DOI: 10.1073/pnas.0603395103.
[4] a) N. Armaroli, V. Balzani, *Angew. Chem. Int. Ed.* **2007**, *46*, 52, DOI: 10.1002/anie.200602373; b) A. Borgschulte, *Front. Ener. Res.* **2016**, *4*, DOI: 10.3389/Fenrg.2016.00011; c) S. Ardo, D. F. Rivas, M. A. Modestino, V. S. Greiving, F. F. Abdi, E. Alarcon Llado, V. Artero, K. Ayers, C. Battaglia, J. P. Becker, D. Bederak, A. Berger, F. Buda, E. Chinello, B. Dam, V. Di Palma, T. Edvinsson, K. Fujii, H. Gardeniers, H. Geerlings, S. M. H. Hashemi, S. Haussener, F. Houle, J. Huskens, B. D. James, K. Konrad, A. Kudo, P. P. Kunturu, D. Lohse, B. Mei, E. L. Miller, G. F. Moore, J. Muller, K. L. Orchard, T. E. Rosser, F. H. Saadi, J. W. Schuttauf, B. Seger, S. W. Sheehan, W. A. Smith, J. Spurgeon, M. H. Tang, R. van de Krol, P. C. K. Vesborg, P. Westerik, *Energ. Environ. Sci.* **2018**, *11*, 2768, DOI: 10.1039/c7ee03639f.
[5] a) M. Carmo, D. L. Fritz, J. Merge, D. Stolten, *Int. J. Hydrogen Energ.* **2013**, *38*, 4901, DOI: 10.1016/j.ijhydene.2013.01.151; b) S. K. Mostafa El-Shafie, Yukio Hayakawa, *J. Pow. Ener. Eng.* **2019**, *7*, 107, DOI: 10.4236/jpee.2019.71007; c) S. Shiva Kumar, V. Himabindu, *Mat. Sci. Ener. Tech.* **2019**, *2*, 442, DOI: 10.1016/j.mset.2019.03.002.
[6] J. H. Russell, L. J. Nuttal, A. P. Fickett, *Abstr. Pap. Am. Chem. Soc.* **1973**, 2.
[7] a) V. S. Thoi, Y. J. Sun, J. R. Long, C. J. Chang, *Chem. Sci. Rev.* **2013**, *42*, 2388, DOI: 10.1039/c2cs35272a; b) M. Wang, L. Chen, L. C. Sun, *Energ. Environ. Sci.* **2012**, *5*, 6763, DOI: 10.1039/c2ee03309g; c) N. Queyriaux, R. T. Jane, J. Massin, V. Artero, M. Chavarot-Kerlidou, *Coord. Chem. Rev.* **2015**, *304*, 3, DOI: 10.1016/j.ccr.2015.03.014; d) W. T. Eckenhoff, *Coord. Chem. Rev.* **2018**, *373*, 295, DOI: 10.1016/j.ccr.2017.11.002; e) S. Fukuzumi, Y. M. Lee, W. Nam, *Coord. Chem. Rev.* **2018**, *355*, 54, DOI: 10.1016/j.ccr.2017.07.014; f) S. Losse, J. G. Vos, S. Rau, *Coord. Chem. Rev.* **2010**, *254*, 2492, DOI: 10.1016/j.ccr.2010.06.004; g) K. E. Dalle, J. Warnan, J. J. Leung, B. Reuillard, I. S. Karmel, E. Reisner, *Chem. Rev.* **2019**, *119*, 2752, DOI: 10.1021/acs.chemrev.8b00392.
[8] a) G. M. Brown, B. S. Brunschwig, C. Creutz, J. F. Endicott, N. Sutin, *J. Am. Chem. Soc.* **1979**, *101*, 1298, DOI: 10.1021/Ja00499a051; b) C. Creutz, H. A. Schwarz, N. Sutin, *J. Am. Chem. Soc.* **1984**, *106*, 3036, DOI: 10.1021/Ja00322a051; c) C. V. Krishnan, B. S. Brunschwig, C. Creutz, N. Sutin, *J. Am. Chem. Soc.* **1985**, *107*, 2005, DOI: 10.1021/Ja00293a035; d) C. V. Krishnan, C. Creutz, D. Mahajan, H. A. Schwarz, N. Sutin, *Isr. J. Chem.* **1982**, *22*, 98; e) C. V. Krishnan, N. Sutin, *J. Am. Chem. Soc.* **1981**, *103*, 2141, DOI: 10.1021/Ja00398a066; f) H. A. Schwarz, C. Creutz, N. Sutin, *Inorg. Chem.* **1985**, *24*, 433, DOI: 10.1021/Ic00197a036; g) J. Hawecker, J. M. Lehn, R. Ziessel, *New J. Chem.* **1983**, *7*, 271; h) J. L. Dempsey, B. S. Brunschwig, J. R. Winkler, H. B. Gray, *Acc. Chem. Res.* **2009**, *42*, 1995, DOI: 10.1021/ar900253e.

[9] a) C. Bachmann, B. Probst, M. Guttentag, R. Alberto, *Chem. Commun*. **2014**, *50*, 6737, DOI: 10.1039/C4CC01500B; b) C. Bachmann, B. Probst, M. Oberholzer, T. Fox, R. Alberto, *Chem. Sci*. **2016**, *7*, 436, DOI: 10.1039/c5sc02124c; c) J. P. Bigi, T. E. Hanna, W. H. Harman, A. Chang, C. J. Chang, *Chem. Commun.* **2010**, *46*, 958, DOI: 10.1039/b915846d; d) M. Guttentag, A. Rodenberg, C. Bachmann, A. Senn, P. Hamm, R. Alberto, *Dalton Trans.* **2013**, *42*, 334, DOI: 10.1039/C2dt31699d; e) E. Joliat, S. Schnidrig, B. Probst, C. Bachmann, B. Spingler, K. K. Baldridge, F. von Rohr, A. Schilling, R. Alberto, *Dalton Trans.* **2016**, *45*, 1737, DOI: 10.1039/c5dt04426j; f) E. Joliat-Wick, N. Weder, D. Klose, C. Bachmann, B. Spingler, B. Probst, R. Alberto, *Inorg. Chem.* **2018**, *57*, 1651, DOI: 10.1021/acs.inorgchem.7b02992; g) J. W. Jurss, R. S. Khnayzer, J. A. Panetier, K. A. El Roz, E. M. Nichols, M. Head-Gordon, J. R. Long, F. N. Castellano, C. J. Chang, *Chem. Sci.* **2015**, *6*, 4954, DOI: 10.1039/c5sc01414j; h) R. S. Khnayzer, V. S. Thoi, M. Nippe, A. E. King, J. W. Jurss, K. A. El Roz, J. R. Long, C. J. Chang, F. N. Castellano, *Energ. Environ. Sci.* **2014**, *7*, 1477, DOI: 10.1039/c3ee43982h; i) M. Nippe, R. S. Khnayzer, J. A. Panetier, D. Z. Zee, B. S. Olaiya, M. Head-Gordon, C. J. Chang, F. N. Castellano, J. R. Long, *Chem. Sci.* **2013**, *4*, 3934, DOI: 10.1039/c3sc51660a; j) S. Schnidrig, C. Bachmann, P. Muller, N. Weder, B. Spingler, E. Joliat-Wick, M. Mosberger, J. Windisch, R. Alberto, B. Probst, *ChemSusChem* **2017**, *10*, 4570, DOI: 10.1002/cssc.201701511; k) Y. J. Sun, J. P. Bigi, N. A. Piro, M. L. Tang, J. R. Long, C. J. Chang, *J. Am. Chem. Soc*. **2011**, *133*, 9212, DOI: 10.1021/ja202743r.

[10] A. Rodenberg, M. Orazietti, B. Probst, C. Bachmann, R. Alberto, K. K. Baldridge, P. Hamm, *Inorg. Chem.* **2015**, *54*, 646, DOI: 10.1021/ic502591a.

[11] A. Rodenberg, M. Orazietti, M. Mosberger, C. Bachmann, B. Probst, R. Alberto, P. Hamm, *ChemPhysChem* **2016**, *17*, 1321, DOI: 10.1002/cphc.201501085.

[12] a) L. P. Tong, A. Kopecky, R. F. Zong, K. J. Gagnon, M. S. G. Ahlquist, R. P. Thummel, *Inorg. Chem*. **2015**, *54*, 7873, DOI: 10.1021/acs.inorgchem.5b00915; b) L. P. Tong, R. F. Zong, R. P. Thummel, *J. Am. Chem. Soc.* **2014**, *136*, 4881, DOI: 10.1021/ja501257d.

[13] D. Shevchenko, M. F. Anderlund, A. Thapper, S. Styring, *Energ. Environ. Sci.* **2011**, *4*, 1284, DOI: 10.1039/c0ee00585a.

[14] a) B. Shan, T. Baine, X. A. N. Ma, X. Zhao, R. H. Schmehl, *Inorg. Chem.* **2013**, *52*, 4853, DOI: 10.1021/ic302381w; b) W. M. Singh, M. Mirmohades, R. T. Jane, T. A. White, L. Hammarstrom, A. Thapper, R. Lomoth, S. Ott, *Chem. Commun.* **2013**, *49*, 8638, DOI: 10.1039/c3cc44655g.

[15] J. Hutter, M. Iannuzzi, F. Schiffmann, J. VandeVondele, *Wires Comput. Mol. Sci.* **2014**, *4*, 15, DOI: 10.1002/wcms.1159.

[16] K. M. Waldie, A. L. Ostericher, M. H. Reineke, A. F. Sasayama, C. P. Kubiak, *Acs Catal.* **2018**, *8*, 1313, DOI: 10.1021/acscatal.7b03396.

[17] S. Goedecker, M. Teter, J. Hutter, *Phys. Rev. B* **1996**, *54*, 1703, DOI: 10.1103/PhysRevB.54.1703.

[18] J. VandeVondele, J. Hutter, *J. Chem. Phys.* **2007**, *127,* DOI: 10.1063/1.2770708.

[19] J. P. Perdew, K. Burke, M. Ernzerhof, *Phys. Rev. Lett.* **1996**, *77*, 3865, DOI: 10.1103/PhysRevLett.77.3865.

[20] R. Sabatini, T. Gorni, S. de Gironcoli, *Phys. Rev. B* **2013**, *87*, DOI: 10.1103/Physrevb.87.041108.

[21] M. Ernzerhof, G. E. Scuseria, *J. Chem. Phys.* **1999**, *110*, 5029, DOI: 10.1063/1.478401.